

Accepted by *The Astrophysical Journal Supplements*.

## The Nature of Composite LINER/H II Galaxies, As Revealed from High-Resolution VLA Observations

Mercedes E. Filho

Lisbon Observatory and Kapteyn Astronomical Institute

Peter D. Barthel

Kapteyn Astronomical Institute

Luis C. Ho

Observatories of the Carnegie Institution of Washington

### ABSTRACT

A sample of 37 nearby galaxies displaying composite LINER/H II and pure H II spectra was observed with the VLA in an investigation of the nature of their weak radio emission. The resulting radio contour maps overlaid on optical galaxy images are presented here, together with an extensive literature list and discussion of the individual galaxies. Radio morphological data permit assessment of the “classical AGN” contribution to the global activity observed in these “transition” LINER galaxies. One in five of the latter objects display clear AGN characteristics: these occur exclusively in bulge-dominated hosts.

*Subject headings:* galaxies: active — galaxies: nuclei — galaxies: Seyfert — radio continuum: galaxies

### 1. Introduction

LINER galaxies are a class of active galaxies characterized by the presence of strong, nuclear, low-ionization emission lines (Heckman 1980). Like Seyfert nuclei, LINERs emit much stronger optical low-ionization forbidden lines compared to H II nuclei, whose line emission is powered by photoionization from young massive stars, but LINERs have a characteristically lower ionization state than Seyferts. In a recent optical survey of nearly 500 nearby galaxies, Ho, Filippenko, & Sargent (1995, 1997a, 1997b) find that  $\sim 20\%$  of all galaxies brighter than  $B_T = 12.5$  mag display LINER-type spectra. An additional 13% of the objects show spectra intermediate between those of “pure” LINERs and “pure” H II nuclei. Ho, Filippenko, & Sargent (1993; see also Ho 1996) dubbed this class as “transition objects,” and they hypothesized that these might be composite

systems in which the optical signal of a weak active nucleus (the LINER component) has been spatially blended by circumnuclear star-forming regions (the H II component).

Models have shown that photoionization by hot stars are able to reproduce the optical spectra of LINERs (Terlevich & Melnick 1985), especially those of the transition-type variety (Shields 1992; Filippenko & Terlevich 1992). Other researchers have advocated shock-wave heating as a viable excitation mechanism for LINERs (Fosbury et al. 1978; Heckman 1980; Dopita & Sutherland 1995). At the same time, an increasing body of evidence suggests that a significant fraction of LINERs do contain irrefutable AGN characteristics (see reviews by Filippenko 1996 and Ho 1999b). Radio surveys, in particular, have shown that many LINERs exhibit weak nuclear radio emission (Heckman 1980; Sadler, Jenkins, & Kotanyi 1989; Wrobel & Heeschen 1991; Slee et al. 1994; Falcke, Wilson, & Ho 1997; Van Dyk & Ho 1998). As discussed in detail by Ho (1999a), weak nuclear radio emission in early-type (elliptical and S0) galaxies is most likely related to accretion-driven energy production in these objects, but at a very low level compared to powerful radio galaxies, which are also usually hosted by early-type systems.

Radio observations provide an especially attractive tool to further our understanding of the LINER phenomenon. Since radio frequencies are not plagued by dust obscuration and photoelectric absorption, high-resolution radio observations potentially offer the cleanest and most efficient method to isolate an AGN core. Although radio emission also arises from supernova remnants and H II regions, AGN cores can be identified through their high degree of central concentration, small angular size, flat spectral indices, and high brightness temperatures.

Given that LINERs are so numerous, they may be the most common type of AGN known. Their large space densities could make a major impact on the faint end of the local AGN luminosity function, which in turn has ramifications for many astrophysical issues ranging from the cosmological evolution of AGN to the contribution of AGN to the cosmic X-ray background. We are therefore conducting high-resolution radio observations of selected LINER samples in order to investigate the interrelation between LINERs and classical AGN. For the present paper — the first in a series — we have concentrated on transition-type LINERs. We report on sensitive Very Large Array (VLA)<sup>1</sup> C-array observations of a sample of 25 such transition LINERs at 8.4 GHz. The resulting images, having angular resolution of about 2''5, allow us to assess the strength and spatial distribution of the nuclear radio emission. For comparison, we have also observed a small sample of 12 pure H II nuclei.

In the following discussion and in upcoming papers, we adopt a Hubble constant of  $H_0 = 75 \text{ km s}^{-1} \text{ Mpc}^{-1}$ .

---

<sup>1</sup>The VLA is a facility of the National Radio Astronomy Observatory (NRAO) which is a facility of the National Science Foundation operated under cooperative agreement by Associated Universities, Inc.

## 2. Sample Selection

The sample of 25 transition LINER/HII galaxies and 12 pure HII nuclei was extracted from the original magnitude-limited Palomar survey of 486 bright northern galaxies (Ho et al. 1995), following the classification criteria outlined in Ho et al. (1997a). The Palomar sample contains 65 transition nuclei (Ho et al. 1997a), from which we chose a subset of 25 that had little or no arcsec-scale resolution radio continuum data published, and that fell within the observation window assigned to us by the VLA. In addition, we selected for comparison a small sample of 12 pure HII nuclei (out of 206 such objects in the full Palomar sample). These were chosen to mimic the Hubble type distribution of the sample of transition objects, again taking into consideration scheduling constraints. We are not aware of any strong biases introduced by our sample selection.

Table 1 lists the 37 sample objects. In addition to the optical positions of the galaxies (columns 3 and 4), this table lists their distance (column 5) and their Hubble type (column 6). The Hubble types and distances are taken from Ho et al. (1997a). The “reference” column (7), together with Table 2, supplies references to earlier radio studies; it is readily apparent that several of the sample objects are well-studied objects, while some are not. We will discuss our observational results in light of these existing data in Section 4. The sample galaxies span a wide range of Hubble types, but the majority are spirals.

– TABLES 1/2: Sample of transition LINER galaxies and HII nuclei –

## 3. Observations and Data Reduction

The resulting sample of 25 composite LINER/HII and 12 pure HII galaxies was observed with the X-band (8.4 GHz) system of the VLA in two observing sessions, on 1997 August 21 and August 25. The array was in its C-configuration, yielding a typical resolution of  $2''.5$ . Two bands of 50 MHz each were combined, yielding a total bandwidth of 100 MHz. Snapshot observations combining two scans of 8–9 minutes each, at different hour angles, were obtained in order to improve the shape of the synthesized beam.

Secondary phase and amplitude calibrators were observed before and after each scan. The primary calibrator was 3C 286, with appropriate baseline constraints, and the adopted 8.4 GHz flux densities, as provided by the VLA staff, were 5.22 Jy and 5.20 Jy, at IF1 and IF2, respectively. The calibration uncertainty is dominated by the uncertainty in the absolute flux density of the primary calibrator, which is a few percent. The array performed well: judging from the calibration sources, the antenna phase and amplitude calibration appeared stable to within a few percent.

The radio data are of high quality, and there was no need for extensive flagging of discrepant points. Reduction of the data was performed using standard NRAO AIPS (version 15OCT98) image processing routines. AIPS task IMAGR was employed to Fourier transform the measured visibilities and obtain CLEAN (Högbom 1974; Clark 1980) maps of the sources. Full-resolution

maps, having synthesized beams of roughly  $2''.5$ , and tapered maps, having beams between about  $5''$  and  $12''$ , were made. This proved useful to detect weak low surface brightness emission. As a rule of thumb,  $1''$  corresponds to 50–100 pc for the typical distances involved. Most images reach the theoretical noise level of  $\sim 0.04$  mJy/beam (Perley, Schwab, & Bridle 1989) to within a factor of two. Self-calibration was employed in the analysis of two of the stronger sources (NGC 4552 and NGC 5354), leading to considerable improvements.

## 4. Results

### 4.1. Radio Maps

Noting that a non-detection should be taken to imply no correlated flux density in excess of 0.5 mJy on the arcsec scale, radio contour maps of the detected galaxies are presented in Figures 1–7, at the end of the paper. The radio maps are overlaid on optical images taken from the Digitized Sky Survey (DSS). In a number of cases only the high-resolution map (typical beamsize  $2''.5$ ) or the low-resolution map (typical beamsize  $7'' - 10''$ ) are shown. Unrelated background radio sources were found in several fields; their number is entirely as expected given the size of the primary beam and the sensitivity of the observations. In cases of large distances from the field center, primary beam corrections were applied. Some of the background sources have been identified using NED (NASA/IPAC Extragalactic Database) and the Cambridge APM (Automatic Plate Measuring) facility. Where possible, we have included them by their name in the tables below. Previously uncatalogued background sources are designated by their sky orientation with respect to the field center for the relevant galaxy. All maps use contouring according to CLEV  $\times (-3, 3, 6, \dots, \text{MLEV})$  mJy/beam where MLEV are powers  $3 \times 2^n$  up to a maximum of 96 and CLEV is the typical noise level on each radio map (see Table 3).

Table 3 lists the various map parameters, with the following column headings: the source name (1), the applied taper (2), the resulting restoring beam (3), the position angle of the beam (4), the image noise level (5), and the relevant figure number (6). The H II nuclei appear at the bottom of the table.

#### – TABLE 3: Radio map parameters –

Given that good phase stability was obtained, as judged from the VLA phase calibrators, the astrometric accuracy of our overlay procedure must be dominated by the DSS accuracy, which is known to be about  $0.6''$  (Véron-Cetty & Véron 1996). This is born out by the images of several unresolved and slightly resolved nuclei (NGC 4552, NGC 5354, NGC 5838, NGC 5846) which appear accurate to within a few tenths of an arcsec.

## 4.2. Comments on Individual Galaxies

With reference to the images in the Appendix, we proceed by discussing the results of our VLA imaging in the light of earlier studies of the sample objects. This discussion also deals with the detected background sources and includes important bibliographic information. We will frequently compare our measurements with sample galaxy flux densities obtained within the VLA 1.4 GHz NVSS and FIRST surveys, having typical resolution of  $45''$  and  $5''$ , respectively (Condon et al. 1998a; Becker, White, & Helfand 1995), as well as with the Green Bank 20 cm and 6 cm surveys, having typical resolution of  $\sim 700''$  and  $3'.5$ , respectively (White & Becker 1992, WB92 hereafter; Becker, White, & Edwards 1991, BWE91 hereafter).

**IC 520 :** No compact structure was seen in this object, not even on the tapered map. It was also not detected in the NVSS. However, Condon (1987) reports a detection at 1.49 GHz: at  $0'.8$  resolution, he measured a 3.1 mJy radio source.

**NGC 2541 :** We did not detect compact structure, not even on the tapered map. This source was also not detected in the FIRST or in the NVSS survey. However, Condon (1987) reports a possible detection at 1.49 GHz,  $0'.8$  resolution, of a 3.2 mJy source, slightly extended to the SW relative to the optical position of the galaxy.

**NGC 2985 :** We detect a 1.9 mJy source. At  $2'.5$  resolution, the source is slightly extended in the N-S direction, along the orientation of the optical galaxy. The tapered map shows a 2.7 mJy core and about 1 mJy weak low surface brightness emission to the SW. The object was also detected in the NVSS: 44.1 mJy. At 1.49 GHz,  $1'.0$  resolution, Condon (1987) measured a total flux of 61.9 mJy: the radio emission of NGC 2985 must be extended over tens of arcseconds.

**NGC 3593 :** On both the untapered and tapered maps we measure about 20 mJy of diffuse,  $45''$  E-W elongated emission, oriented along the major axis of the host of this HII nucleus. NVSS measured 87 mJy emission, WB92 measured 132 mJy (hence the radio source exceeds one arcminute in size), whereas BWE91 measured 53 mJy. The 1.4 GHz,  $5''$  resolution map of Condon et al. (1990) shows an E-W oriented source of 63.4 mJy: these and our VLA data imply a steep-spectrum radio source.

We also detect an unrelated 10.6 mJy source,  $3'$  to the N, extended towards the E. As judged from the APM survey, the POSS plates show an as yet unclassified nonstellar source at this position: background source NGC 3593N is most likely a weak distant radio galaxy.

**NGC 3627, M 66 :** This interacting galaxy belongs to the Leo triplet. The 8.4 GHz maps show a  $2'$  triple source aligned with the inner bar of the optical galaxy. The outer radio components are related to star formation in the disk of the galaxy (Urbanik, Gräve, & Klein 1985). We measure 3.9 mJy integrated emission in the compact central component, while  $\sim 25$  mJy are distributed in the NW and SE components. From comparison with low-resolution surveys (NVSS: 324.9 mJy; WB92: 434 mJy; BWE91: 141 mJy) we infer that most of the radio emission of this steep-spectrum radio source is resolved out by our observations. The triple radio structure was

also observed by Saikia et al. (1994), at 5 GHz with 2'' resolution. Combining our data with the Saikia et al. (1994) and the Hummel et al. (1987) data, we conclude that the nuclear radio source in NGC3627 must be of variable, flat-spectrum nature. More recently, high resolution (0.''15) 15 GHz observations detected an unresolved 1.4 mJy core (N. Nagar, private communication).

**NGC 3628 :** Like NGC 3627, this galaxy also belongs to the Leo triplet. Our 8.4 GHz full-resolution map shows some extended emission to the N and an eastern extension that is roughly aligned with the projected disk of the galaxy. The nuclear region is clearly resolved. The total flux density on our low-resolution map is about 70 mJy, 70% of which is in  $\sim 15''$  diffuse emission. The NVSS measured 292 mJy whereas WB92, at lower resolution, detected 402 mJy, indicating resolved large-scale emission. At 1.4 GHz Condon et al. (1990) measured 203 mJy and 205 mJy at 5'' and 1.''5 resolution, respectively. These and our data imply a steep-spectrum radio source, in agreement with the results from the Effelsberg 100m telescope (Schlickeiser, Werner, & Wielebinski 1984). Carral, Turner, & Ho (1990) observed this object at 15 GHz using the VLA in A-array and measured a total flux of 23 mJy. These authors sampled the innermost part of the source and obtain a  $\sim 4''$  string of a dozen components aligned with the major axis of the galaxy, that they suggest could be star-forming regions in the disk.

**NGC 3675 :** We detect about 1.5 mJy of low surface brightness emission on our tapered maps. NVSS detected a 48.9 mJy source, whereas FIRST measured 8.04 mJy: the source must be strongly resolved. 1.49 GHz VLA D-array observations (Condon 1987; Gioia & Fabbiano 1987) detected a  $\sim 50$  mJy source, oriented N-S, along the major axis of the optical galaxy. Condon, Frayer, & Broderick (1991) report a flux density of 27 mJy at 4.85 GHz and a steep spectral index between 4.8 and 1.4 GHz.

**NGC 3681 :** We did not detect a radio source on the untapered or tapered maps. In contrast, NVSS measured a weak source of about 4.2 mJy – at much lower resolution.

**NGC 3684 :** This HII nucleus had no radio source detected, either on the untapered or on the tapered maps, but NVSS detected a 15.9 mJy source. The radio emission of NGC 3684 must be diffuse.

We do, however, detect a partially resolved 18.1 mJy background source, 3' to the SW, which APM identifies with a 19.5 mag stellar-like object. Further identification is still lacking.

**NGC 4013 :** We detect a moderately resolved 1.1 mJy core and a small extension to the NE, parallel to the projected disk of this edge-on galaxy. There is an additional 3 mJy of weak disk emission. On the basis of the widely different NVSS and FIRST detections (40.5 vs. 11.9 mJy), this disk emission must extend tens of arcseconds. Hummel, Beck, & Dettmar (1991) present 10'' resolution 5 GHz data of NGC 4013 (UGC 6963) which show both the prominent core and the extended disk emission. Recent high resolution (0.''15) 15 GHz observations did not detect NGC 4013 above a  $10\sigma$  limit of 1 mJy (N. Nagar, private communication).

We also detect a slightly resolved 3.8 mJy background source, 2' to the far SE. This source is

also clearly seen in the map of Condon (1987). The APM facility reveals a 19.6 mag stellar-like object, which lacks further identification as yet.

**NGC 4100 :** We detect about 7 mJy of low surface brightness emission associated with this H II nucleus. The tapered map shows a slight extension to the SE along the major axis of the optical galaxy. NVSS detected a 50.3 mJy source and FIRST detected 17.8 mJy, indicating resolution effects.

**NGC 4217 :** We detect about 22 mJy, distributed along  $\sim 1'.5$  of the projected galactic disk of this H II nucleus. From low-resolution observations (NVSS: 123 mJy; WB92: 139 mJy; BWE91: 40 mJy) we conclude that NGC 4217 harbours extended low surface brightness radio emission, which must have a steep radio spectrum.

**NGC 4245 :** No radio source associated with this H II nucleus was detected on the untapered or tapered maps. Neither NVSS nor FIRST has detected this object at 1.4 GHz.

**NGC 4321, M 100 :** We detect about 16 mJy of low surface brightness emission in the nuclear region of this well-known grand design spiral in the Virgo cluster. The tapered map shows emission slightly extended to the NW. NVSS detected 87 mJy, while WB92 measured 323 mJy and BWE91 87 mJy. At 1.49 GHz,  $0'.9$  resolution Condon (1987) measured 180 mJy total flux in a  $\sim 3' \times 2'$  region. At 4.9 GHz,  $1'.5$  resolution Collison et al. (1994) detect a ring-like structure coincident with our main feature. At 8.5 GHz,  $0'.2$  resolution, these authors detect two unresolved sources, having peaks of 0.37 mJy/beam (E) and 0.22 mJy/beam (W), respectively. The eastern radio source is coincident with their 4.9 GHz main component while the one to the W is coincident with the optical nucleus and has a flat spectrum (Collison et al. 1994).

We also detect an unresolved source,  $1.5'$  to the SE, with 1.3 mJy integrated flux, apparently located near the middle of the southern spiral arm of the galaxy. It is clearly visible on the NGC 4321 map. We have identified this object with SN 1979C (Weiler et al. 1981). Collison et al. (1994) measured 2 mJy for this SN 1979C, at 4.9 GHz.

**NGC 4369, Mrk 439 :** We detect 3.8 mJy of low surface brightness disk emission associated with this H II nucleus. On the basis of widely different NVSS and FIRST detections (24.3 vs. 4.67 mJy), this disk emission must extend over tens of arcsec. The Condon et al. (1990) 1.49 GHz image, at  $15''$  resolution, shows a 18.3 mJy source with extended emission to the E.

**NGC 4405, IC 788 :** No compact emission was detected in the untapered or tapered maps. NVSS detected weak (4.5 mJy) emission for this H II galaxy.

We did, however, detect a partially resolved 10.1 mJy source,  $2'$  SW of the NGC 4405 target position. As judged from the APM, the POSS plates show a 19.2 mag stellar-like object at this position, which we subsequently identify as the  $z = 1.929$  QSO, LBQS 1223+1626 (e.g., Hewett, Foltz, & Chaffee 1995).

**NGC 4414 :** We detect  $\sim 29$  mJy of low surface brightness emission, distributed along  $\sim 1'.5$ ,

in a structure aligned with the galaxy’s major axis. NVSS detected a 242 mJy source while FIRST detected a double-peaked source with 44 and 64 mJy components. The Condon (1983), 1.465 GHz, 12.5'' resolution map and the Condon (1987), 1.49 GHz, 1.0' resolution map show comparable N-S structure, measuring  $\sim 0.22$  Jy. Using this last value plus the 78 mJy measured at 4.85 GHz, 15'' resolution, Condon et al. (1991) obtain a steep spectral index.

**NGC 4424 :** On the tapered map we detect a resolved  $\sim 1$  mJy core plus 1.5 mJy weak low surface brightness emission to the E along the projected disk of this candidate merger galaxy (Kenney et al. 1996). NVSS detected a weak 4.5 mJy source. Our full-resolution data show the core of this H II nucleus to be somewhat resolved. This is borne out of our recent high resolution (0.25') 8.4 GHz observations which did not detect NGC 4424 above a  $3\sigma$  limit of 0.2 mJy.

We also detect an unrelated, slightly resolved 13.3 mJy source, 2.5' to the SE. The APM identifies it with a 20.2 mag stellar-like object. Further properties of this background source remain as yet unknown.

**NGC 4470 :** We detect  $\sim 3$  mJy of weak low surface brightness emission, extending 30'' along the galaxy major axis. NVSS detected 17.1 mJy associated with this H II nucleus.

We also detect an unrelated, resolved 16.0 mJy radio source, 1.5' to the NE of NGC 4470, which is not identified on the POSS plate (APM). We identify this object with the radio source TXS 1227+081 (Douglas et al. 1996), which has as yet no optical identification.

**NGC 4552, M 89 :** We detect about 77 mJy in a strong core plus possibly a jet-like structure to the NE. NVSS detected a 103 mJy source. Since BWE91 measured 64 mJy at 5 GHz, the radio source in NGC 4552 must have a relatively flat radio spectrum, which is in agreement with findings by Condon et al. (1991). The radio source appears to be variable (Wrobel & Heeschen 1984; Ekers, Fanti, & Miley 1983; Sramek 1975a, 1975b; Ekers & Ekers 1973). Our recent subarcsec resolution 8.4 GHz images have confirmed this object’s compactness.

**NGC 4643 :** No compact radio structure was detected on the untapered or the tapered maps. NVSS also did not detect this source. However, we have detected several very weak sources ( $\sim 1$  mJy) on the tapered maps, some of which may be due to weak diffuse disk emission.

**NGC 4710 :** We detect about 6 mJy of weak disk emission associated with this H II nucleus. NVSS measured a 19.3 mJy source. At 1.49 GHz, Condon et al. (1990) measure 17.2 mJy and 14.7 mJy at 15 and 5'' resolution, respectively. The data imply a resolved steep-spectrum radio source.

We also detect a 4.8 mJy resolved background source, 2.5' to the E of NGC 4710. No identification could be found on the POSS.

**NGC 4713 :** We detect  $\sim 1.2$  mJy weak low surface brightness disk emission on our tapered maps. NVSS measured a 46.9 mJy source: our observations must have resolved out much of the flux.

**NGC 4800** : We detect about 1.2 mJy of weak low surface brightness emission, stretching  $\sim 30''$  along the galaxy major axis. NVSS detected a 23.5 mJy source and FIRST 12.2 mJy. Therefore, our observations are resolving out much of the emission of this HII nucleus.

**NGC 4826 , M 64**: We detect about 21 mJy of low surface brightness emission. The central region on the full-resolution map (not presented here) shows a double-peaked component, which can be compared to the complex inner triple structure of the 15 and 5 GHz,  $2''$  resolution maps of Turner & Ho (1994). Combining the data indicates that this is a steep spectrum source. NVSS detected a 101 mJy source and BWE91 detected a 56 mJy source. The 1.49 GHz,  $1'.0$  resolution data of Condon et al. (1998b) and Condon (1987) show a  $\sim 100$  mJy source, as do the data of Gioia & Fabbiano (1987) at  $40''$  resolution.

**NGC 4845** : On our tapered maps we detect a 2 mJy core and some emission to the N, perpendicular to the galaxy major axis, plus 10 mJy of  $\sim 20''$  elongated disk emission. NVSS detected a 43.8 mJy source associated with this HII nucleus. The data of Condon et al. (1990) imply resolution effects on the 10 arcsec scale.

**NGC 5012** : We detect some very weak ( $\sim 1$  mJy) features near the target phase center. NVSS detected a 31.4 mJy source, but as FIRST did not detect it, we must be dealing with extended low surface brightness emission.

**NGC 5354** : We detect an unresolved 11.7 mJy core. NVSS and FIRST detected a 8.4 and 8.0 mJy source, respectively, implying that the NGC 5354 radio source is unresolved at a resolution of  $5''$ . The 4.85 GHz,  $15''$  resolution maps of Condon et al. (1991) show 7 mJy emission, implying that the nuclear radio source has an inverted spectrum. Our recent subarcsec resolution 8.4 GHz images have confirmed this object's compactness.

Paired galaxy NGC 5353 is also detected,  $1'.25$  to the S, with a 26.7 mJy core. Condon et al. (1991) measure 29 mJy at 4.85 GHz,  $15''$  resolution, implying that NGC 5353 also hosts a flat spectrum radio source.

**NGC 5656** : We detect  $\sim 1$  mJy of weak low surface brightness emission, stretching over  $\sim 25''$  along the major axis of the galaxy. NVSS detected a 22 mJy source.

**NGC 5678** : We detect about 8.5 mJy of low surface brightness emission stretching over  $\sim 1'.2$  along the major axis of the galaxy. The tapered map shows what could be a double-peaked source, similar to the  $6''$  resolution, 1.4 GHz map of Condon (1983). NVSS detected a 112 mJy source while BWE91 measured 68 mJy. The NVSS and BWE91 results, combined with Condon (1983) reporting 109 mJy at 1.4 GHz, imply a steep spectrum source.

**NGC 5838** : We have detected a slightly resolved 2.2 mJy source. NVSS detected 3.0 mJy, while Wrobel & Heeschen (1991) report a 2 mJy source (5 GHz,  $5''$  resolution): the nuclear radio source in NGC 5838 must have a flat radio spectrum. Our recent subarcsec resolution 8.4 GHz images have confirmed this object's compactness.

There is also an unrelated, unresolved 1.3 mJy source, about  $1'.5$  to the S of NGC 5838. The POSS plates reveal an 18.4 mag star-like object at that position, for which as yet no redshift is available.

**NGC 5846 :** We have detected a partially resolved 7.1 mJy source. NVSS measured a 22 mJy source. 1.4 GHz VLA observations by Möllenhoff, Hummel, & Bender (1992) measured an unresolved core of 9 mJy plus 10 mJy of additional diffuse emission: NGC 5846 must possess a compact flat-spectrum core component. Our recent subarcsec resolution 8.4 GHz images have confirmed this object's compactness.

**NGC 5879 :** No radio structure was detected on the untapered or the tapered maps. NVSS detected a 21 mJy source, which hence must arise in an extended low surface brightness region.

However, we did detect a 292.1 mJy, slightly resolved background source, about  $2'$  NE of our target. It shows up only on the POSS red plate as a noise-like source. We have identified this source as QSO 1508+5714, at a redshift of 4.301 (Hook et al. 1995). It is in the WENSS (Rengelink et al. 1997) and in BWE91 (282 mJy) as well as in WB92 (149 mJy). Patnaik et al. (1992) have observed the source with the VLA A-array at 8.5 GHz and measured 153 mJy: 1508+5714 must be a variable flat-spectrum quasar.

**NGC 5921 :** We have detected a very weak 0.5 mJy core and some additional weak extended emission. At 1.49 GHz and  $0'.9$  resolution, Condon (1987) measured a 20.8 mJy source with an additional 2.8 mJy eastern component which we do not detect at 8.4 GHz. All emission must be of low surface brightness nature.

**NGC 6384 :** Following the NVSS non-detection, we also do not detect (compact) radio emission from NGC 6384. However, Condon (1987), at 1.49 GHz and  $1'.2$  resolution, found the radio source, having  $\sim 35$  mJy, to be very extended.

**NGC 6482 :** We have not detected this source at 8.4 GHz and neither did NVSS.

We did, however, detect a slightly resolved 23.6 mJy background source, about  $3'$  to the S of NGC 6482. On the full-resolution map this source is slightly extended. The POSS plates show a 20.9 mag stellar object. We have identified this source with the radio source 1749+2302 included in GB6, with 26 mJy flux density.

**NGC 6503 :** We do not detect radio emission from this galaxy on the full-resolution or on the tapered maps. 1.4 GHz data (NVSS and Condon 1987) indicate a NW-SE extended  $\sim 40$  mJy source, which consequently must be diffuse.

We also detect a background source, about  $6'$  to the SW. Due to the large distance from the phase center, which implies a large and uncertain primary beam correction, we cannot assess the flux density of this source. The source appears as a 16.9 mag stellar-like object on the POSS plates. We have identified this object with the BL Lacertae source 1749+701 at redshift 0.77 (Hughes, Aller, & Aller 1992). This object has been extensively observed at other radio-frequencies and is

included in the WENSS (Rengelink et al. 1997) as well as BWE91 and WB92. The only other 8.5 GHz measurement of this source comes from Patnaik et al. (1992). They measure 558 mJy with the VLA A-array.

Table 4 summarizes the properties of the background sources, including the previously identified, as well as the new, identifications. Tabulated 8.4 GHz fluxes have been corrected for primary beam attenuation.

– **TABLE 4: Field/background sources** –

### 4.3. Radio Source Parameters

For each galaxy with a 8.4 GHz detection, we list in Table 5 the radio source parameters, measured both from the full-resolution and the tapered maps. Peak and integrated values (columns 3 and 6), as well as sky positions of bidimensional gaussian fits (columns 4 and 5) are tabulated. These values were obtained using the AIPS task IMFIT. As we are often dealing with resolved and/or asymmetric emission, such measurements are often inaccurate and must represent lower limits. In such cases, we have estimated the integrated 8.4 GHz flux density from inspection of the map and the relevant clean component file and we have given it the prefix “ $\geq$ ” (column 6). Also, given the fact that we have fitted single gaussian to the brightest source components, the accuracy of the radio peak positions is judged to be  $\lesssim 1''$  (see images). For NGC 3627, the quoted peak and integrated value are of the central core. In parentheses we include the total flux of the three components (see Section 4.2).

– **TABLE 5: Radio parameters of detected sources** –

From a quick comparison with the integrated NVSS 1.4 GHz flux densities, it is found that in many cases the high-resolution observations must have resolved a substantial fraction of the emission. This can be quantified by examination of the spectral index values. Table 6 lists spectral indices  $\alpha_{1.4}^{8.4}$  ( $S_\nu \propto \nu^{-\alpha}$ ) (column 5), obtained by combining the NVSS flux densities (column 2) and the integrated 8.4 GHz flux densities (column 3) taken from Table 5. Due to the fact that the NVSS beam (45'') exceeds the 8.4 GHz beam (7'–10'') by a substantial factor, these spectral index values should be considered as upper limits. It indeed appears that in most of these cases the radio emission was documented to be extended over tens of arcseconds. We also compile calculated NVSS radio luminosities (column 4) for the 37 galaxies under consideration. Again, for NGC 3627 quoted values refer to the compact core except when in parentheses, in which case the values refer to all three source components.

– **TABLE 6: summary** –

Most sample galaxies are seen to display steep spectral indices, as commonly found for star-forming late-type galaxies (Condon 1992). The following objects have flat ( $\alpha \leq 0.6$ ) spectra: NGC 4552, NGC 5354, NGC 5838 and NGC 5846 and the H II nucleus in NGC 4424. We will return

to this issue in the next Section.

## 5. Discussion

Our VLA imaging observations have yielded X-band detections of 27 of the 37 sample galaxies. These 27 include NGC 4643 and NGC 5012, which were marginally detected. As for the non-detections, they are equally distributed over the transition LINERs and the H II nuclei. It appears that non-detection at X-band, at a resolution of  $2''.5$ – $12''$ , correlates with 1.4 GHz (NVSS) weakness and/or low surface brightness. Table 6 indicates that the NVSS radio luminosity distributions of the subsamples are comparable. The integrated 1.4 GHz radio luminosities imply that the sample sources span the usual luminosity range for nearby galaxies ( $10^{26} - 10^{30.5}$  erg s $^{-1}$  Hz $^{-1}$ ; see, e.g., Condon 1987, 1992). With the exception of NGC 4424 (see Section 4.2), none of the H II nuclei display compact nuclear emission and/or a flat radio spectrum. This is in strong contrast to the transition LINER galaxies.

Purely based on the radio morphology, the transition LINER objects can be divided into two categories. The first is made up of galaxies displaying extended, steep-spectrum, low surface brightness radio emission, usually tracing the optical isophotes of the host galaxy. The second category refers to objects that, in addition to extended emission, also show compact nuclear radio emission. The first category displays radio morphologies that are consistent with their being due to large-scale star formation; in several cases the radio morphology is seen to trace the H II regions in the host. However, we stress that the presence of a very weak nuclear component in these objects may still be masked by the more dominant radio emission from star-forming regions. The second category, which we will refer to in the following as AGN candidates, is comprised of NGC 3627, NGC 4552, NGC 5354, NGC 5838, and NGC 5846. The last four of these are characterized with a flat radio spectral index between 1.4 and 8.4 GHz (see end of Section 4.3). Judging from high-resolution observations which isolate the nuclear emission, the compact nucleus of NGC 3627 also displays a flat radio spectrum (see Section 4.2). These AGN candidates are on average more luminous than the non-AGN and, as we shall see below, their hosts are early rather than late-type galaxies. While at first sight the H II nucleus NGC 4424 also belongs in this AGN candidate class, the radio image (Fig. 3d) shows it to be resolved. Higher resolution observations recently carried out by us indeed resolve all the nuclear emission in NGC 4424 (see Section 4.2), in contrast to the AGN candidates from the transition LINER sample. As such there is a clear separation between the non-AGN and AGN candidate classes.

Apparently, galaxies with composite LINER and star-formation spectra separate out into objects with and without a clear signature of an AGN, that is to say, a compact, flat-spectrum radio source. The prime question to address, of course, is whether the optical spectra of these classes differ in any way. Deferring the full analysis of this issue to another paper, we here just note that the class of AGN candidates indeed displays somewhat stronger [N II] and [S II] lines in their optical spectra. As we will demonstrate in the forthcoming paper in this series, the behavior

of the so called  $u$ -parameter, which measures the radio/far-IR ratio, also supports the weak AGN classification. However, like in the case of Seyfert galaxies showing a  $\sim 30\%$  incidence rate of compact radio cores (e.g., Norris et al. 1990), there is not a one-to-one correspondence between compact radio emission and nuclear activity. We conclude that the radio properties permit to isolate AGN candidates among the sample of transition LINERs, although the absence of radio cores cannot be used to argue against their being AGN. These conclusions strongly support the hypothesis which resulted from the VLA observations of transition LINER NGC 7331 by Cowan et al. (1994).

Inspection of Table 6 readily shows that these AGN candidates are hosted by rather early-type galaxies (E–Sb). The relevant radio core luminosities  $L_{8.4\text{GHz}}$  range from  $\sim 10^{26.2} - 10^{28.5} \text{ erg s}^{-1} \text{ Hz}^{-1}$ , which is several orders of magnitude less than the core luminosities in FRI or FRII type (Fanaroff & Riley 1974) radio galaxies and quasars, and in the range of the weakest radio cores in Seyfert galaxies (Giuricin et al. 1996). This, then, implies that weak LINER AGN preferentially occur in bulge-dominated hosts, not necessarily just in ellipticals, consistent with statistical results from other lines of evidence (Ho et al. 1997b; Ho 1999b). This is in agreement with the case of Seyfert galaxies, for which the radio core emission was also found to be stronger in early-type hosts (Giuricin et al. 1996). As such, these weak AGN differ from the more powerful FRI radio galaxies, which are commonly associated with elliptical galaxies, not seldom brightest cluster galaxies (Zirbel & Baum 1995). They exceed the very weak nuclear source in the nearby transition LINER NGC 7331 (Cowan et al. 1994) by a factor of  $\sim 15$ , and are comparable in strength to the well-known variable radio core of the LINER nucleus in M 81 (e.g., Ho et al. 1999). Hence, it must be concluded that at least some weak LINER AGN reveal themselves by low-power radio cores. This supports the analysis of Ho (1999a), who proposed that the weak nuclear radio sources (radio power  $10^{26} - 10^{29} \text{ erg s}^{-1} \text{ Hz}^{-1}$ ) in nearby elliptical and S0 galaxies are the low-luminosity counterparts of more powerful AGN.

Finally, it is intriguing that the transition LINER in the elliptical galaxy NGC 6482 remained undetected in our observations (as well as in the NVSS). Given that NGC 6482 is the most distant object in our sample, our non-detection would still allow a  $\leq 10^{27} \text{ erg s}^{-1} \text{ Hz}^{-1}$  compact radio source to reside in this object.

Full analysis of our sample, including optical emission-line and infrared luminosities, will be presented in forthcoming papers. To address the physical origin behind the findings presented here will be the challenge for future work.

## 6. Conclusions

A sample of composite LINER/HII galaxies and pure HII nuclei was studied using the VLA (C-array) at 8.4 GHz. On the basis of their radio morphological properties, the composite sources can be divided into objects with low surface brightness emission confined mainly to the plane of

the galaxy and objects displaying compact nuclear components. The former objects are similar in radio morphology to the HII nuclei in our sample, whereas the latter show morphologies consistent with AGN. All five of the LINER AGN are hosted by bulge-dominated galaxies (Hubble type E–Sb), and four of them show flat spectral indices between 8.4 and 1.4 GHz. In terms of radio luminosity, the present LINER AGN populate the range of low core radio luminosities, which implies that classical AGN of low luminosity exist in a wide range of galaxy types.

M. E. F. is supported by grant PRAXIS XXI/BD/15830/98 from the Fundação para a Ciência e Tecnologia, Ministério da Ciência e Tecnologia, Portugal. P. D. B. acknowledges a visitor’s grant from the Space Telescope Science Institute, where a large part of this paper could be written. L. C. H. is partly funded by NASA grant NAG 5-3556, and by NASA grants GO-06837.01-95A and AR-07527.02-96A from the Space Telescope Science Institute (operated by AURA, Inc., under NASA contract NAS5-26555). We want to thank Neil Nagar for providing us with some of his preliminary results.

This research was supported in part by the European Commission TMR Programme, Research Network Contract ERBFMRXCT96-0034 “CERES.” We made extensive use of the APM (Automatic Plate Measuring) Facility, run by the Institute of Astronomy in Cambridge, the STScI DSS (Digitized Sky Survey), produced under US government grant NAGW – 2166, and NED (NASA/IPAC Extragalactic Database), which is operated by the Jet Propulsion Laboratory, California Institute of Technology, under contract with NASA.

## REFERENCES

- Becker, R. H., White, R. L., & Edwards, A. L. 1991, *ApJS*, 75, 1
- Becker, R. H., White, R. L., & Helfand, D. J. 1995, *ApJ*, 450, 559
- Carral, P., Turner, J. L., & Ho, P. T. P. 1990, *ApJ*, 362, 434
- Clark, B. G., 1980, *A&A*, 89, 377
- Collison, P. M., Saikia, D. J., Pedlar, A., Axon, D. J., & Unger, S. W. 1994, *MNRAS*, 268, 203
- Condon, J. J. 1983, *ApJS*, 53, 459
- Condon, J. J. 1987, *ApJS*, 63, 485
- Condon, J. J. 1992, *ARA&A*, 30, 575
- Condon, J. J., & Broderick, J. J. 1988, *AJ*, 96, 30
- Condon, J. J., Condon, M. A., Gisler, G., & Puschell, J. J. 1982, *ApJ*, 252, 102
- Condon, J. J., Cotton, W. D., Greisen, E. W., Yin, Q. F., Perley, R. A., Taylor, G. B., & Broderick, J. J. 1998a, *AJ*, 115, 1693
- Condon, J. J., Frayer, D. T., & Broderick, J. J. 1991, *AJ*, 101, 362

- Condon, J. J., Helou, G., Sanders, D. B., & Soifer, B. T. 1990, *ApJS*, 73, 359
- Condon, J. J., Yin, Q. F., Thuan, T. X., & Boller, Th. 1998b, *AJ*, 116, 2682
- Cowan, J. J., Romanishin, W., & Branch, D. 1994, *ApJ*, 436, L139
- Dopita, M. A., & Sutherland, R. S. 1995, *ApJ*, 102, 161
- Douglas, J. N., Bash, F. N., Bozayan, F. A., Torrence, G. W., & Wolfe, C. 1996, *AJ*, 111, 1945
- Dressel, L. L., & Condon, J. J. 1978, *ApJS*, 36, 53
- Dumke, M. K., Krause, M., Wielebinski, R., & Klein, U. 1995, *A&A*, 302, 691
- Ekers, R. D., & Ekers, J. A. 1973, *A&A*, 24, 247
- Ekers, R. D., Fanti, R., & Miley, G. K. 1983, *A&A*, 120, 297
- Fabbiano, G., Gioia, I. M., & Trinchieri, G. 1989, *ApJ*, 347, 127
- Falcke, H., Wilson, A. S., & Ho, L. C. 1997, in *Relativistic Jets in AGN*, ed. M. Sikora & M. Ostrowski, 13
- Fanaroff, B. L., & Riley, J. M. 1974, *MNRAS*, 167, 31P
- Filippenko, A. V. 1996, in *The Physics of LINERs in View of Recent Observations*, ed. M. Eracleous et al. (San Francisco: ASP), 17
- Filippenko, A. V., & Terlevich, R. 1992, *ApJ*, 397, L79
- Fosbury, R. A. E., Melbold, U., Goss, W. M., & Dopita, M. A. 1978, *MNRAS*, 183, 549
- Gioia, I. M., & Fabbiano, G. 1987, *ApJS*, 63, 771
- Giuricin, G., Fadda, D., & Mezzetti, M. 1996, *ApJ*, 468, 475
- Gregory, P. C., & Condon, J. J. 1991, *ApJS*, 75, 1011
- Haynes, M., & Sramek, R. A. 1975, *AJ*, 80, 673
- Heckman, T. M. 1980, *A&A*, 87, 152
- Heckman, T. M., Balick, B., & Crane, P. C. 1980, *A&AS*, 40, 295
- Hewett, P. C., Foltz, C. B., & Chaffee, F. H. 1995, *AJ*, 109, 1498
- Ho, L. C. 1996, in *The Physics of LINERs in View of Recent Observations*, ed. M. Eracleous et al. (San Francisco: ASP), 103
- Ho, L. C. 1999a, *ApJ*, 510, 631
- Ho, L. C. 1999b, *Advances in Space Research*, 23 (5-6), 813
- Ho, L. C., Filippenko, A. V., & Sargent, W. L. W. 1993, *ApJ*, 417, 63
- Ho, L. C., Filippenko, A. V., & Sargent, W. L. W. 1995, *ApJS*, 98, 477
- Ho, L. C., Filippenko, A. V., & Sargent, W. L. W. 1997a, *ApJS*, 112, 315
- Ho, L. C., Filippenko, A. V., & Sargent, W. L. W. 1997b, *ApJ*, 487, 568

- Ho, L. C., Van Dyk, S. D., Pooley, G. G., Sramek, R. A., & Weiler, K. W. 1999, *AJ*, 118, 843
- Högbom, J. A., 1974, *A&AS*, 15, 417
- Hook, I. M., McMahon, R. G., Patnaik, A. R., Browne, I. W. A., Wilkinson, P. N., Irwin, M. J., & Hazard, C. 1995, *MNRAS*, 273, L63
- Hughes, P. A., Aller, H. D., & Aller, M. F. 1992, *ApJ*, 396, 469
- Hummel, E. 1980, *A&AS*, 41, 151
- Hummel, E., Beck, R., & Dettmar, R.-J. 1991, *A&AS*, 87, 309
- Hummel, E., & Kotanyi, C. G. 1982, *A&A*, 106, 183
- Hummel, E., van der Hulst, J. M., Keel, W. C., & Kennicutt, R. C., Jr. 1987, *A&AS*, 70, 517
- Jenkins, C. R. 1982, *MNRAS*, 200, 705
- Jones, D. L., Terzian, Y., & Sramek, R. A. 1981a, *ApJ*, 246, 28
- Jones, D. L., Terzian, Y., & Sramek, R. A. 1981b, *ApJ*, 247, L57
- Kenney, J. D. P., Koopmann, R. A., Rubin, V. C., & Young, J. S. 1996, *AJ*, 111, 152
- Klein, U., & Emerson, D. T. 1981, *A&A*, 94, 29
- Möllenhoff, C., Hummel, E., & Bender, R. 1992, *A&A*, 255, 35
- Niklas, S., Klein, U., Braine, J., & Wielebinski, R. 1995, *A&AS*, 114, 21
- Norris, R. P., Allen, D. A., Sramek, R. A., Kesteven, M. J., & Troup, E. R. 1990, *ApJ*, 359, 291
- Patnaik, A. R., Browne, I. W. A., Wilkinson, P. N., & Wrobel, J. M. 1992, *MNRAS*, 254, 655
- Perley, R. A., Schwab, F. R., & Bridle, A. H. 1989, in *Synthesis Imaging in Radio Astronomy: A Collection of Lectures from the Third NRAO Synthesis Imaging Summer School* (San Francisco: ASP), 6
- Rengelink, R. B., Tang, Y., de Bruyn, A. G., Miley, G. K., Bremer, M. N., Röttgering, H. J. A., & Bremer, M. A. R. 1997, *A&AS*, 124, 259
- Reuter, H.-P., Krause, M., Wielebinski, R., & Lesch, H. 1991, *A&A*, 248, 12
- Sadler, E. M., Jenkins, C. R., & Kotanyi, C. G. 1989, *MNRAS*, 240, 591
- Saikia, D. J., Pedlar, A., Unger, S. W., & Axon, D. J. 1994, *MNRAS*, 270, 46
- Schlickeiser, R., Werner, W., & Wielebinski, R. 1984, *A&A*, 140, 227
- Shields, J. C. 1992, *ApJ*, 399, L27
- Slee, O. B., Sadler, E. M., Reynolds, J. E., & Ekers, R. D. 1994, *MNRAS*, 269, 928
- Sramek, R. A. 1975a, *AJ*, 80, 771
- Sramek, R. A. 1975b, *ApJ*, 198, L13
- Terlevich, R., & Melnick, J. 1985, *MNRAS*, 213, 841

- Turner, K. C., Helou, G., & Terzian, Y. 1988, *PASP*, 100, 452
- Turner, J. L., & Ho, P. T. P. 1994, *ApJ*, 421, 122
- Urbanik, M., Gräve, R., & Klein, U. 1985, *A&A*, 152, 291
- Urbanik, M., Klein, U., & Gräve, R. 1986, *A&A*, 166, 107
- van Breugel, W. J. M., Schilizzi, R. T., Hummel, E., & Kapahi, V. K. 1981, *A&A*, 96, 310
- van der Hulst, J. M., Crane, & P. C., Keel, W. C. 1981, *AJ*, 86, 1175
- van der Kruit, P. C. 1973a, *A&A*, 29, 231
- van der Kruit, P. C. 1973b, *A&A*, 29, 249
- Van Dyk, S. D., & Ho, L. C. 1998, in *IAU Symp. 184, The Central Regions of the Galaxy and Galaxies*, ed. Y. Sofue (Dordrecht: Kluwer), 489
- Véron-Cetty, M.-P., & Véron, P. 1996, *A&AS*, 115, 97
- Vila, M. B., Pedlar, A., Davies, R. D., Hummel, E., & Axon, D. J. 1990, *MNRAS*, 242, 379
- Weiler, K. W., van der Hulst, J. M., Sramek, R. A., & Panagia, N. 1981, *ApJ*, 243, L151
- White, R. L., & Becker, R. J. 1992, *ApJS*, 79, 331
- Wrobel, J. M., & Heeschen, D. S. 1984, *ApJ*, 287, 41
- Wrobel, J. M., & Heeschen, D. S. 1991, *AJ*, 101, 148
- Zirbel, E. L., & Baum, S. A. 1995, *ApJ*, 448, 521

| Galaxy   | Other name | R.A.(J2000)<br><i>h m s</i> | Dec(J2000)<br><i>° ' "</i> | D<br>Mpc | Hubble Type      | Reference   |
|----------|------------|-----------------------------|----------------------------|----------|------------------|---|
| IC 520   |            | 08 53 42.3                  | +73 29 29                  | 47.0     | SAB(rs)ab?       | 26  |
| NGC 2541 |            | 08 14 40.2                  | +49 03 42                  | 10.6     | SA(s)cd          | 26,41   |
| NGC 2985 |            | 09 50 20.9                  | +72 16 44                  | 22.4     | (R')SA(rs)ab     | 1,2,5,26,41,42  |
| NGC 3627 | M 66       | 11 20 14.9                  | +12 59 21                  | 6.6      | SAB(s)b          | 1,5,6,11,13,14<br>17,24,26,28,41,44                         |
| NGC 3628 |            | 11 20 16.2                  | +13 35 22                  | 7.7      | SAb pec spin     | 1,4,5,11,13,14,16<br>17,18,19,24,26,30<br>34,36,38,41,44,45 |
| NGC 3675 |            | 11 26 08.0                  | +43 34 58                  | 12.8     | SA(s)b           | 1,3,17,25,26,41<br>42,47                                    |
| NGC 3681 |            | 11 26 29.4                  | +16 51 51                  | 24.2     | SAB(r)bc         | 1   |
| NGC 4013 |            | 11 58 31.1                  | +43 56 50                  | 17.0     | SAb spin         | 1,3,15,26,41  |
| NGC 4321 | M 100      | 12 22 54.8                  | +15 49 20                  | 16.8     | SAB(s)bc         | 1,5,7,11,13,14,17<br>18,20,22,24,26,27<br>35,36,41,47       |
| NGC 4414 |            | 12 26 27.2                  | +31 13 24                  | 16.8     | SA(rs)c?         | 1,3,5,11,13,14<br>17,18,24,26,31,36                         |
| NGC 4552 | M 89       | 12 35 39.9                  | +12 33 25                  | 9.7      | E                | 1,13,14,17,22,29<br>37,38,39,41,43,44                       |
| NGC 4643 |            | 12 43 20.2                  | +01 58 41                  | 16.8     | SB(rs)0/a        | 21,24,41  |
| NGC 4713 |            | 12 49 57.8                  | +05 18 39                  | 25.7     | SAB(rs)d         | 1   |
| NGC 4826 | M 64       | 12 56 44.2                  | +21 41 05                  | 17.9     | (R)SA(rs)ab      | 1,2,8,13,14,17,24,25<br>26,36,40,41,44,46                   |
| NGC 5012 |            | 13 11 36.8                  | +22 54 56                  | 4.1      | SAB(rs)c         | 1   |
| NGC 5354 |            | 13 53 26.7                  | +40 18 09                  | 32.8     | SA0 spin         | 1,3,12,17,32,41,44  |
| NGC 5656 |            | 14 30 25.5                  | +35 19 17                  | 42.6     | SAab             | 1   |
| NGC 5678 |            | 14 32 05.2                  | +57 55 23                  | 35.6     | SAB(rs)b         | 1,13,14,17,18,31  |
| NGC 5838 |            | 15 05 26.5                  | +02 06 01                  | 28.5     | SA0 <sup>-</sup> | 1   |
| NGC 5846 |            | 15 06 29.2                  | +01 36 21                  | 28.5     | E0 <sup>-</sup>  | 1,9,10,12,41  |
| NGC 5879 |            | 15 09 47.1                  | +57 00 05                  | 16.8     | SA(rs)bc?        | 1,41  |
| NGC 5921 |            | 15 21 56.3                  | +05 04 11                  | 25.2     | SB(r)bc          | 1,24,26,41  |
| NGC 6384 |            | 17 32 24.5                  | +07 03 37                  | 26.6     | SAB(r)bc         | 5,17,24,26,41   |
| NGC 6482 |            | 17 51 48.9                  | +23 04 20                  | 52.3     | E:               | ...   |
| NGC 6503 |            | 17 49 27.5                  | +70 08 41                  | 6.1      | SA(s)cd          | 1,5,26,41,42  |

Table 1: Sample sources – the 25 transition LINERs.

| Galaxy   | Other name | R.A.(J2000)<br><i>h m s</i> | Dec(J2000)<br><i>° ' "</i> | D<br>Mpc | Hubble Type   | Reference                         |
|----------|------------|-----------------------------|----------------------------|----------|---------------|-----------------------------------|
| NGC 3593 |            | 11 14 36.0                  | +12 49 06                  | 5.5      | SA(S)0/a:     | 1,5,11,13,14,17<br>18,24,26,33,41 |
| NGC 3684 |            | 11 27 11.1                  | +17 01 49                  | 23.4     | SA(rs)bc      | 1                                 |
| NGC 4100 |            | 12 06 08.1                  | +49 34 59                  | 17.0     | (R')SA(rs)bc  | 1,3,5,26,41,42                    |
| NGC 4217 |            | 12 15 50.7                  | +47 05 37                  | 17.0     | SAb spin      | 1,3,5,11,13,14<br>15,17,26,41     |
| NGC 4245 |            | 12 17 36.7                  | +29 36 29                  | 9.7      | SB(r)0/a      | ...                               |
| NGC 4369 | Mrk 439    | 12 24 36.1                  | +39 22 58                  | 21.6     | (R)SA(rs)a    | 1,3,18,41                         |
| NGC 4405 | IC 788     | 12 26 07.1                  | +16 10 51                  | 31.5     | SA(rs)0:      | 1                                 |
| NGC 4424 |            | 12 27 11.4                  | +09 25 15                  | 16.8     | SA(s)a:       | 1                                 |
| NGC 4470 |            | 12 29 37.9                  | +07 49 25                  | 31.4     | Sa ?          | 1                                 |
| NGC 4710 |            | 12 49 38.9                  | +15 09 55                  | 16.8     | SA(r)0+? spin | 1,12,15,18,32,36<br>41,43         |
| NGC 4800 |            | 12 54 38.0                  | +46 31 52                  | 15.2     | SA(rs)b       | 1,3,41                            |
| NGC 4845 |            | 12 58 01.3                  | +01 34 30                  | 15.6     | SA(s)ab spin  | 1,18                              |

Table 1: Sample sources – the 12 H II nuclei (cont.).

| No. | Reference               | No. | Reference                 |
|-----|-------------------------|-----|---------------------------|
| 1   | Condon et al. 1998a     | 25  | Gioia & Fabbiano 1987     |
| 2   | Condon et al. 1998b     | 26  | Condon 1987               |
| 3   | Becker et al. 1995      | 27  | Urbanik et al. 1986       |
| 4   | Dumke et al. 1995       | 28  | Urbanik et al. 1985       |
| 5   | Niklas et al. 1995      | 29  | Wrobel & Heeschen 1984    |
| 6   | Saikia et al. 1994      | 30  | Schlickeiser et al. 1984  |
| 7   | Collison et al. 1994    | 31  | Condon 1983               |
| 8   | Turner & Ho 1994        | 32  | Hummel & Kotanyi 1982     |
| 9   | Slee et al. 1994        | 33  | Jenkins et al. 1982       |
| 10  | Möllenhoff et al. 1992  | 34  | Condon et al. 1982        |
| 11  | White & Becker 1992     | 35  | Weiler et al. 1981        |
| 12  | Wrobel & Heeschen 1991  | 36  | van der Hulst et al. 1981 |
| 13  | Becker et al. 1991      | 37  | van Breugel et al. 1981   |
| 14  | Gregory & Condon 1991   | 38  | Jones et al. 1981a        |
| 15  | Hummel et al. 1991      | 39  | Jones et al. 1981b        |
| 16  | Reuter et al. 1991      | 40  | Klein & Emerson 1981      |
| 17  | Condon et al. 1991      | 41  | Hummel et al. 1980        |
| 18  | Condon et al. 1990      | 42  | Heckman et al. 1980       |
| 19  | Carral et al. 1990      | 43  | Dressel & Condon 1978     |
| 20  | Vila et al. 1990        | 44  | Sramek 1975a              |
| 21  | Fabbiano et al. 1989    | 45  | Haynes & Sramek 1975      |
| 22  | Turner et al. 1988      | 46  | van der Kruit 1973a       |
| 23  | Condon & Broderick 1988 | 47  | van der Kruit 1973b       |
| 24  | Hummel et al. 1987      |     |                           |

Table 2: References for the radio data (see Table 1).

| Galaxy   | Taper<br>K $\lambda$ | Beamsize<br>arcsec <sup>2</sup> | PA<br>° | <i>rms</i><br>mJy/beam | Fig. No. |
|----------|----------------------|---------------------------------|---------|------------------------|----------|
| NGC 2985 | 0                    | 2.98 × 2.15                     | −7.19   | 0.08                   | 1a       |
|          | 20                   | 9.30 × 7.20                     | −84.28  | 0.09                   |          |
| NGC 3627 | 0                    | 2.55 × 2.29                     | −25.24  | 0.10                   | 1c       |
|          | 15                   | 10.96 × 9.93                    | −64.54  | 0.25                   |          |
| NGC 3628 | 0                    | 2.54 × 2.30                     | −14.68  | 0.45                   | 1d       |
|          | 20                   | 8.78 × 7.48                     | −76.82  | 0.80                   |          |
| NGC 3675 | 25                   | 7.27 × 5.81                     | 71.04   | 0.09                   | 2a       |
| NGC 4013 | 0                    | 2.52 × 2.26                     | −19.39  | 0.07                   | 2b       |
|          | 30                   | 5.90 × 5.26                     | 77.17   | 0.09                   |          |
| NGC 4321 | 0                    | 2.52 × 2.33                     | −11.27  | 0.07                   | 3a       |
|          | 30                   | 7.25 × 5.14                     | −89.95  | 0.08                   |          |
| NGC 4414 | 0                    | 2.43 × 2.32                     | −37.18  | 0.08                   | 3c       |
|          | 10                   | 18.70 × 17.70                   | −62.41  | 0.15                   |          |
| NGC 4552 | 0                    | 2.93 × 2.54                     | 11.27   | 0.08                   | 4b       |
| NGC 4643 | 15                   | 12.04 × 11.13                   | 52.57   | 0.07                   | 4c       |
| NGC 4713 | 15                   | 12.12 × 10.95                   | 44.22   | 0.08                   | 5a       |
| NGC 4826 | 0                    | 2.76 × 2.29                     | −6.23   | 0.08                   | 5c       |
|          | 20                   | 9.62 × 8.26                     | 62.33   | 0.10                   |          |
| NGC 5012 | 15                   | 11.59 × 11.18                   | 74.66   | 0.08                   | 6a       |
| NGC 5354 | 0                    | 2.84 × 2.37                     | −42.75  | 0.06                   | 6b       |
| NGC 5656 | 20                   | 9.54 × 8.39                     | 75.33   | 0.08                   | 6c       |
| NGC 5678 | 0                    | 2.99 × 2.21                     | −27.47  | 0.07                   | 6d       |
|          | 15                   | 11.09 × 10.75                   | −34.43  | 0.10                   |          |
| NGC 5838 | 0                    | 3.13 × 2.43                     | 1.94    | 0.07                   | 7a       |
|          | 35                   | 5.62 × 5.23                     | 51.83   | 0.07                   |          |
| NGC 5846 | 0                    | 3.13 × 2.49                     | 3.94    | 0.07                   | 7b       |
|          | 30                   | 7.06 × 5.67                     | 68.01   | 0.07                   |          |
| NGC 5921 | 20                   | 7.12 × 5.63                     | 67.8    | 0.06                   | 7c       |

| Galaxy   | Taper<br>K $\lambda$ | Beamsize<br>arcsec <sup>2</sup> | PA<br>° | <i>rms</i><br>mJy/beam | Fig. No. |
|----------|----------------------|---------------------------------|---------|------------------------|----------|
| NGC 3593 | 0                    | 2.58 × 2.36                     | −17.94  | 0.09                   | 1b       |
|          | 20                   | 9.70 × 7.17                     | −80.16  | 0.15                   |          |
| NGC 4100 | 0                    | 2.61 × 2.35                     | −29.79  | 0.07                   | 2c       |
|          | 20                   | 7.83 × 7.40                     | 84.07   | 0.08                   |          |
| NGC 4217 | 20                   | 7.30 × 5.41                     | 76.75   | 0.09                   | 2d       |
| NGC 4369 | 0                    | 2.48 × 2.34                     | −14.62  | 0.07                   | 3b       |
|          | 30                   | 6.94 × 5.51                     | 88.71   | 0.10                   |          |
| NGC 4424 | 0                    | 3.00 × 2.46                     | 12.14   | 0.09                   | 3d       |
|          | 30                   | 7.21 × 5.60                     | 76.27   | 0.07                   |          |
| NGC 4470 | 15                   | 9.95 × 7.99                     | 59.70   | 0.07                   | 4a       |
| NGC 4710 | 0                    | 2.86 × 2.48                     | 3.88    | 0.10                   | 4d       |
|          | 30                   | 5.50 × 5.16                     | 72.46   | 0.08                   |          |
| NGC 4800 | 30                   | 5.28 × 5.15                     | −82.56  | 0.10                   | 5b       |
| NGC 4845 | 0                    | 3.27 × 2.44                     | 15.08   | 0.08                   | 5d       |
|          | 30                   | 7.08 × 5.69                     | 64.51   | 0.10                   |          |

Table 3: Map parameters of the detected sources. The H II nuclei appear below the transition LINERs.

| Field Source   | R.A.(J2000)<br><i>h m s</i> | Dec(J2000)<br><i>° ' "</i> | z      | NVSS<br>mJy | $F_{8.4}^{\text{int}}$<br>mJy | $\alpha_{1.4}^{8.4}$ | Reference             |
|----------------|-----------------------------|----------------------------|--------|-------------|-------------------------------|----------------------|-----------------------|
| NGC 3593N      | 11 14 37.20                 | +12 52 15.0                | ...    | 18.7        | 10.6                          | 0.3                  | ...                   |
| NGC 3684SW     | 11 27 02.42                 | +16 58 34.8                | ...    | 41.4        | 18.1                          | 0.5                  | ...                   |
| NGC 4013SE     | 11 58 38.61                 | +43 55 05.5                | ...    | ...         | 3.8                           | ...                  | ...                   |
| SN 1979C       | 12 22 58.67                 | +15 47 51.6                | 0.0052 | ...         | 1.3                           | ...                  | Weiler et al. 1981    |
| LBQS 1223+1626 | 12 25 59.09                 | +16 10 21.2                | 1.9290 | 8.9         | 10.1                          | -0.1                 | Hewett et al. 1995    |
| NGC 4424SE     | 12 27 19.83                 | +09 23 03.0                | ...    | 11.0        | 13.3                          | -0.1                 | ...                   |
| TXS 1227+081   | 12 29 47.64                 | +07 50 26.7                | ...    | 110.9       | 16.0                          | 1.1                  | Douglas et al. 1996   |
| NGC 4710E      | 12 49 48.63                 | +15 09 33.3                | ...    | 4.1         | 4.8                           | -0.1                 | ...                   |
| NGC 5353       | 13 53 26.69                 | +40 16 58.7                | 0.0077 | 41.0        | 26.7                          | 0.2                  | Hummel & Kotanyi 1982 |
| NGC 5838S      | 12 05 28.11                 | +02 04 16.2                | ...    | 7.5         | 1.3                           | 1.0                  | ...                   |
| 87GB 1508+5714 | 15 10 02.97                 | +57 02 43.6                | 4.3010 | 202.4       | 292.1                         | -0.2                 | Hook et al. 1995      |
| 87GB 1749+2302 | 17 51 49.10                 | +23 01 26.7                | 0.7700 | 45.3        | 23.6                          | 0.4                  | Becker et al. 1991    |
| BL 1749+701    | 17 48 32.87                 | +70 05 52.5                | ...    | 735.6       | ...                           | ...                  | Hughes et al. 1992    |

Table 4: The field source parameters. The integrated 8.4 GHz flux densities (column 6) have been corrected for primary beam attenuation.

| Galaxy   | Taper<br>K $\lambda$ | F <sub>max</sub><br>mJy/beam | R.A.(J2000)<br>h m s | Dec(J2000)<br>° ' " | F <sub>int</sub><br>mJy |
|----------|----------------------|------------------------------|----------------------|---------------------|-------------------------|
| NGC 2985 | 0                    | 1.07                         | 09 50 22.1           | +72 16 44           | ≥1.9                    |
|          | 20                   | 1.30                         | 09 50 22.0           | +72 16 44           | ≥2.7                    |
| NGC 3627 | 0                    | 1.30                         | 11 20 15.0           | +12 59 30           | 3.7 (≥22.1)             |
|          | 15                   | 2.99                         | 11 20 15.1           | +12 59 31           | 3.9 (≥25.7)             |
| NGC 3628 | 0                    | 15.31                        | 11 20 17.0           | +13 35 20           | 61.4                    |
|          | 20                   | 41.07                        | 11 20 17.0           | +13 35 19           | 69.1                    |
| NGC 3675 | 25                   | 0.37                         | 11 26 08.7           | +43 35 01           | ≥1.3                    |
| NGC 4013 | 0                    | 1.08                         | 11 58 31.4           | +43 56 51           | ≥3.8                    |
|          | 30                   | 2.28                         | 11 58 31.4           | +43 56 51           | ≥4.1                    |
| NGC 4321 | 0                    | 0.34                         | 12 22 55.4           | +15 49 21           | 7.5                     |
|          | 30                   | 1.64                         | 12 22 55.3           | +15 49 21           | 15.7                    |
| NGC 4414 | 0                    | 0.65                         | 12 26 27.5           | +31 13 40           | 2.3                     |
|          | 10                   | 3.72                         | 12 26 26.7           | +31 13 42           | 29.4                    |
| NGC 4552 | 0                    | 76.51                        | 12 35 39.8           | +12 33 23           | 76.8                    |
| NGC 4643 | 15                   | ...                          | ...                  | ...                 | ~1                      |
| NGC 4713 | 15                   | 0.32                         | 12 49 58.4           | +05 18 39           | ≥1.2                    |
| NGC 4826 | 0                    | 1.8                          | 12 56 43.4           | +21 41 01           | 18.9                    |
|          | 20                   | 4.03                         | 12 56 43.7           | +21 41 00           | 21.1                    |
| NGC 5012 | 15                   | ...                          | ...                  | ...                 | ~1                      |
| NGC 5354 | 0                    | 11.61                        | 13 53 26.7           | +40 18 10           | 11.7                    |
| NGC 5656 | 20                   | 0.40                         | 14 30 26.9           | +35 19 25           | ≥0.7                    |
| NGC 5678 | 0                    | 0.74                         | 14 32 05.9           | +57 54 51           | ≥2.0                    |
|          | 15                   | 1.31                         | 14 32 05.5           | +57 54 51           | ≥8.6                    |
| NGC 5838 | 0                    | 1.85                         | 15 05 26.3           | +02 05 57           | 2.1                     |
|          | 35                   | 1.88                         | 15 05 26.3           | +02 05 57           | 2.2                     |
| NGC 5846 | 0                    | 6.03                         | 15 06 29.3           | +01 36 21           | 6.4                     |
|          | 30                   | 6.36                         | 15 06 29.3           | +01 36 21           | 7.1                     |
| NGC 5921 | 20                   | 0.46                         | 15 21 56.4           | +05 04 14           | ≥0.8                    |

| Galaxy   | Taper<br>K $\lambda$ | F <sub>max</sub><br>mJy/beam | R.A.(J2000)<br>h m s | Dec(J2000)<br>° ' " | F <sub>int</sub><br>mJy |
|----------|----------------------|------------------------------|----------------------|---------------------|-------------------------|
| NGC 3593 | 0                    | 1.82                         | 11 14 36.4           | +12 49 06           | 16.4                    |
|          | 20                   | 4.79                         | 11 14 36.6           | +12 49 05           | 20.0                    |
| NGC 4100 | 0                    | 0.93                         | 12 06 08.6           | +49 34 58           | ≥3.9                    |
|          | 20                   | 3.58                         | 12 06 08.4           | +49 34 59           | ≥7.3                    |
| NGC 4217 | 20                   | 0.55                         | 12 15 51.0           | +47 05 29           | ≥22.0                   |
| NGC 4369 | 0                    | 0.31                         | 12 24 36.3           | +39 22 56           | 1.3                     |
|          | 30                   | 1.31                         | 12 24 36.3           | +39 22 57           | 3.8                     |
| NGC 4424 | 0                    | 0.60                         | 12 27 11.2           | +09 25 17           | 2.0                     |
|          | 30                   | 0.80                         | 12 27 11.7           | +09 25 17           | 2.5                     |
| NGC 4470 | 15                   | 0.38                         | 12 29 37.8           | +07 49 24           | ≥2.6                    |
| NGC 4710 | 0                    | 0.71                         | 12 49 38.9           | +15 09 59           | ≥6.0                    |
|          | 30                   | 1.64                         | 12 49 39.0           | +15 09 58           | 6.1                     |
| NGC 4800 | 30                   | 0.36                         | 12 54 37.8           | +46 31 52           | ≥1.2                    |
| NGC 4845 | 0                    | 1.76                         | 12 58 01.2           | +01 34 32           | ≥9.9                    |
|          | 30                   | 5.15                         | 12 58 01.1           | +01 34 32           | 12.5                    |

Table 5: The 8.4 GHz radio parameters of the detected sources. The H II nuclei appear below the transition LINERs.

| Galaxy   | NVSS<br>mJy | $F_{8.4}^{\text{int}}$<br>mJy | $\text{Log } L_{1.4}^{\text{tot}}$<br>$\text{erg s}^{-1} \text{ Hz}^{-1}$ | $\alpha_{1.4}^{8.4}$ | Hubble Type      |
|----------|-------------|-------------------------------|---|----------------------|------------------|
| IC 520   | ...         | ...                           | ...   | ...                  | SAB(rs)ab?       |
| NGC 2541 | ...         | ...                           | ...   | ...                  | SA(s)cd          |
| NGC 2985 | 44.1        | 2.7                           | 28.4  | 1.6                  | (R')SA(rs)ab     |
| NGC 3627 | 324.9       | 3.9 (25.7)                    | 28.2  | 2.5 (1.5)            | SAB(s)b          |
| NGC 3628 | 291.7       | 69.1                          | 28.3  | 0.8                  | SAb pec spin     |
| NGC 3675 | 48.9        | 1.3                           | 27.9  | 2.0                  | SA(s)b           |
| NGC 3681 | 4.2         | ...                           | 27.5  | ...                  | SAB(r)bc         |
| NGC 4013 | 40.5        | 4.1                           | 28.2  | 1.3                  | SAb spin         |
| NGC 4321 | 87.1        | 15.7                          | 28.5  | 1.0                  | SAB(s)bc         |
| NGC 4414 | 242.2       | 29.4                          | 28.4  | 1.2                  | SA(rs)c?         |
| NGC 4552 | 103.1       | 76.8                          | 28.5  | 0.2                  | E                |
| NGC 4643 | ...         | $\sim 1$                      | ...   | ...                  | SB(rs)0/a        |
| NGC 4713 | 46.9        | 1.2                           | 28.3  | 2.0                  | SAB(rs)d         |
| NGC 4826 | 101.1       | 21.1                          | 27.3  | 0.9                  | (R)SA(rs)ab      |
| NGC 5012 | 31.4        | $\sim 1$                      | 28.8  | ...                  | SAB(rs)c         |
| NGC 5354 | 8.4         | 11.7                          | 28.0  | -0.2                 | SA0 spin         |
| NGC 5656 | 22.0        | 0.7                           | 28.7  | 2.0                  | SAab             |
| NGC 5678 | 111.5       | 8.6                           | 29.2  | 1.4                  | SAB(rs)b         |
| NGC 5838 | 3.0         | 2.2                           | 27.5  | 0.2                  | SA0 <sup>-</sup> |
| NGC 5846 | 22.1        | 7.1                           | 28.3  | 0.6                  | E0 <sup>-</sup>  |
| NGC 5879 | 21.1        | ...                           | 27.9  | ...                  | SA(rs)bc?        |
| NGC 5921 | 24.2        | 0.8                           | 28.3  | 1.9                  | SB(r)bc          |
| NGC 6384 | ...         | ...                           | ...   | ...                  | SAB(r)bc         |
| NGC 6482 | ...         | ...                           | ...   | ...                  | E:               |
| NGC 6503 | 40.0        | ...                           | 27.3  | ...                  | SA(s)cd          |
| Galaxy   | NVSS<br>mJy | $F_{8.4}^{\text{int}}$<br>mJy | $\text{Log } L_{1.4}^{\text{tot}}$<br>$\text{erg s}^{-1} \text{ Hz}^{-1}$ | $\alpha_{1.4}^{8.4}$ | Hubble Type      |
| NGC 3593 | 87.3        | 20.0                          | 27.5  | 0.8                  | SA(S)0/a:        |
| NGC 3684 | 15.9        | ...                           | 28.0  | ...                  | SA(rs)bc         |
| NGC 4100 | 50.3        | 7.3                           | 28.2  | 1.1                  | (R')SA(rs)bc     |
| NGC 4217 | 122.8       | 22.0                          | 28.6  | 1.0                  | SAb spin         |
| NGC 4245 | ...         | ...                           | ...   | ...                  | SB(r)0/a         |
| NGC 4369 | 24.3        | 3.8                           | 28.1  | 1.0                  | (R)SA(rs)a       |
| NGC 4405 | 4.5         | ...                           | 27.7  | ...                  | SA(rs)0:         |
| NGC 4424 | 4.5         | 2.5                           | 27.2  | 0.3                  | SA(s)a:          |
| NGC 4470 | 17.1        | 2.6                           | 28.3  | 1.1                  | Sa ?             |
| NGC 4710 | 19.3        | 6.1                           | 27.8  | 0.7                  | SA(r)0+? spin    |
| NGC 4800 | 23.5        | 1.2                           | 27.8  | 1.7                  | SA(rs)b          |
| NGC 4845 | 43.8        | 12.5                          | 28.1  | 0.7                  | SA(s)ab spin     |

Table 6: Summary of the detected sources. The HII nuclei appear below the transition LINERs. All tabulated spectral index values are upper limits (see Section 4.3).

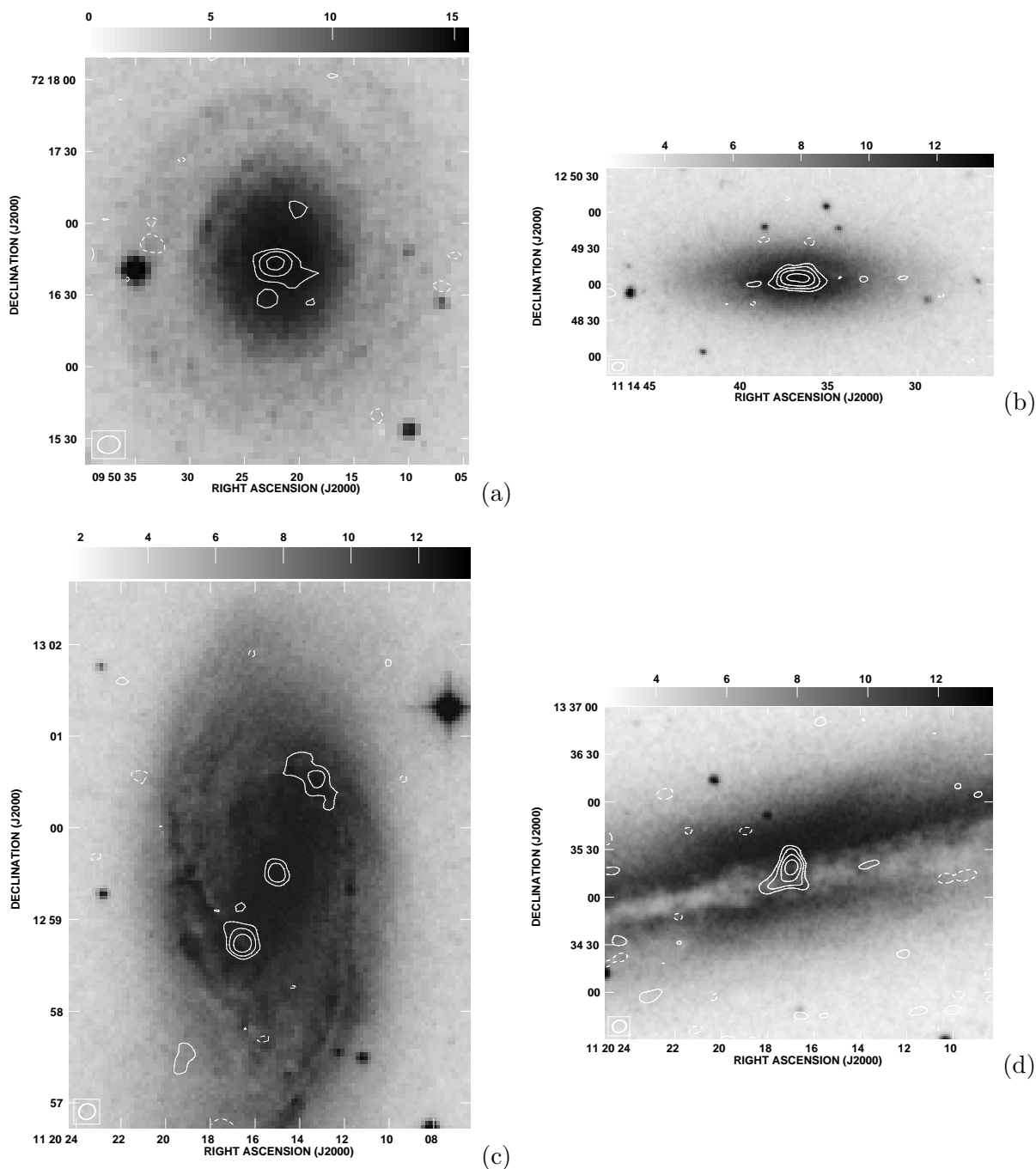


Fig. 1.— Radio emission (contours) superimposed on optical images from the Digitized Sky Survey (greyscale). Contour levels are  $\text{CLEV} \times (-3, 3, 6, 12, 24, 48, 96)$ , where  $\text{CLEV}$  is the  $rms$  noise level (see Table 3). The grey scale levels are arbitrary. The size of the restoring beam is given in parentheses after each object name (see Table 3). (a) NGC 2985 ( $9''.30 \times 7''.20$ ), (b) NGC 3593 ( $9''.70 \times 7''.17$ ), (c) NGC 3627 ( $10''.96 \times 9''.93$ ) and (d) NGC 3628 ( $8''.78 \times 7''.48$ ). NGC 3593 is an H II nucleus.

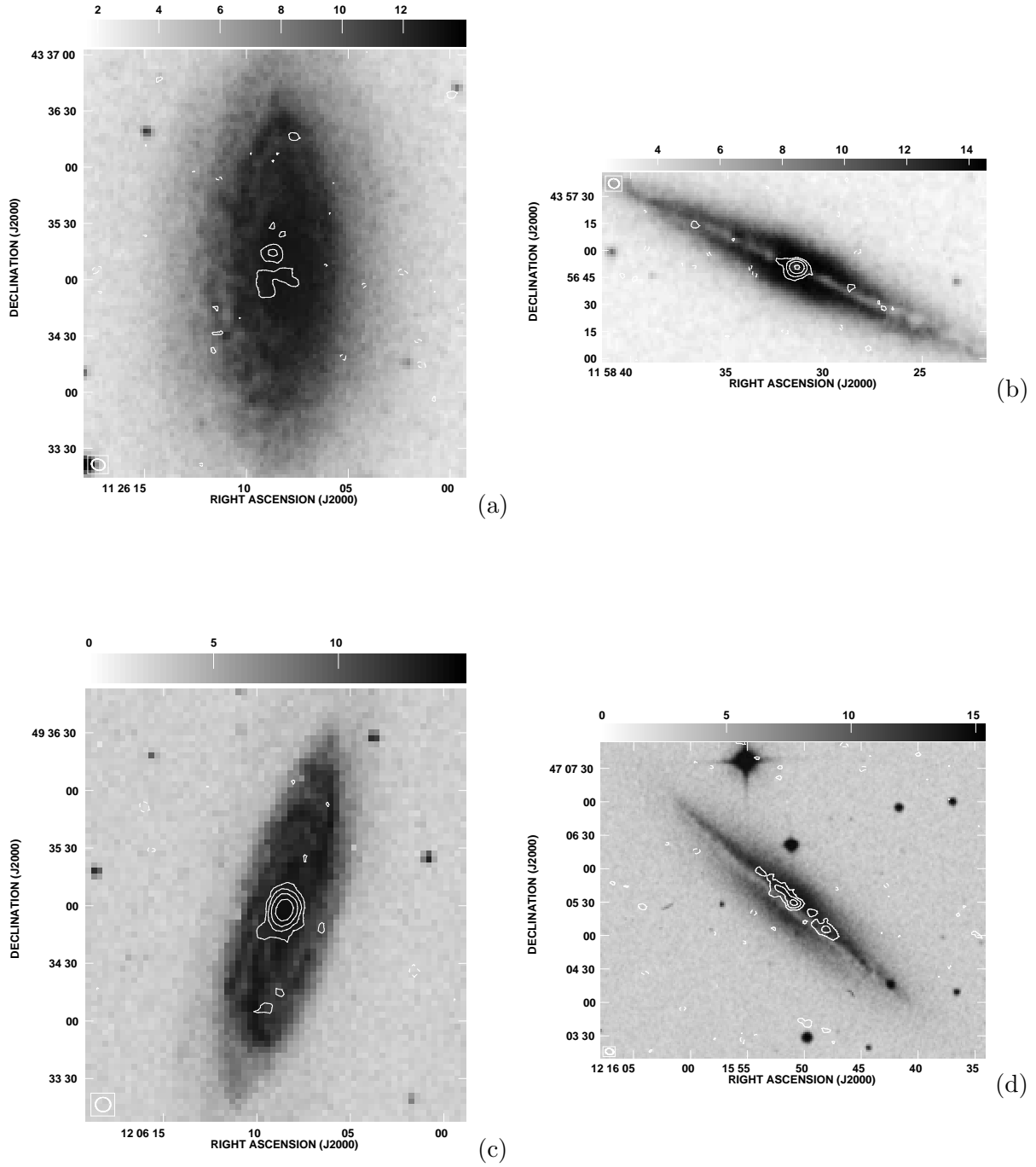


Fig. 2.— As in Figure 1. (a) NGC 3675 ( $7''.27 \times 5''.81$ ), (b) NGC 4013 ( $5''.90 \times 5''.26$ ), (c) NGC 4100 ( $7''.83 \times 7''.40$ ) and (d) NGC 4217 ( $7''.30 \times 5''.41$ ). NGC 4100 and NGC 4217 are H II nuclei.

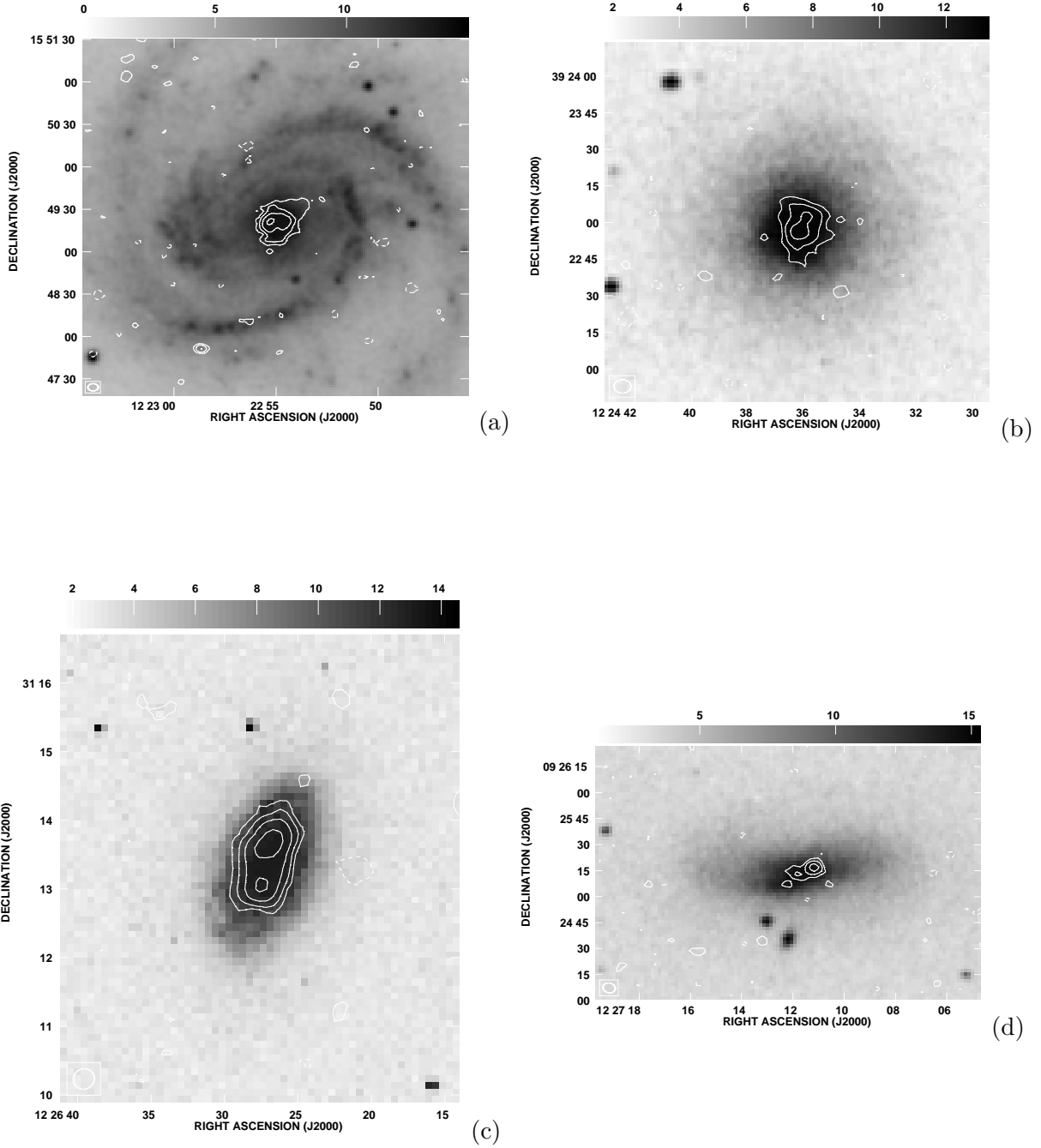


Fig. 3.— As in Figure 1. (a) NGC 4321 ( $7''.25 \times 5''.14$ ), (b) NGC 4369 ( $6''.94 \times 5''.51$ ), (c) NGC 4414 ( $18''.17 \times 17''.70$ ) and (d) NGC 4424 ( $7''.21 \times 5''.60$ ). NGC 4369 and NGC 4424 are H II nuclei.

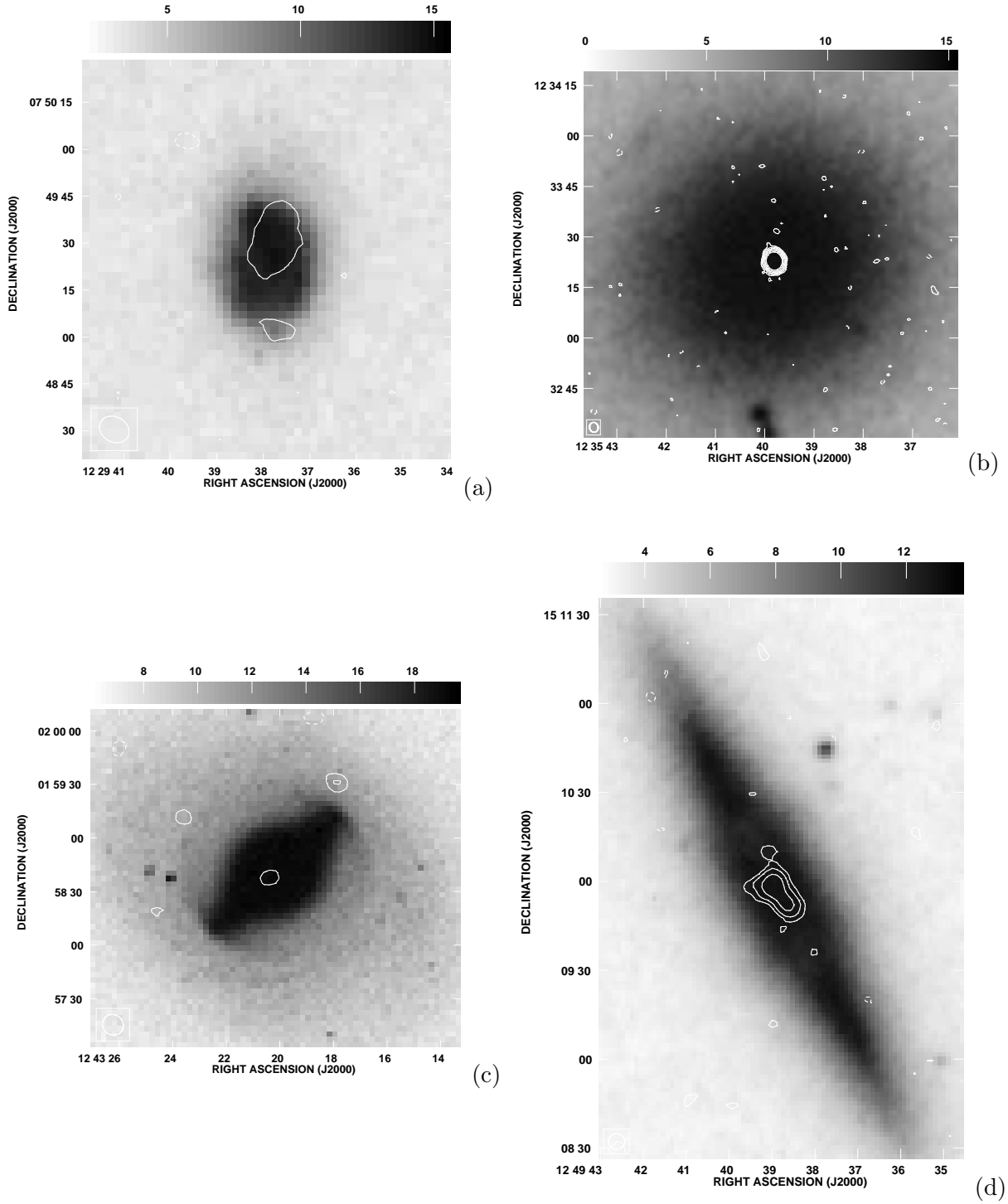


Fig. 4.— As in Figure 1. (a) NGC 4470 ( $9''.95 \times 7''.99$ ), (b) NGC 4552 ( $2''.93 \times 2''.54$ ), (c) NGC 4643 ( $12''.04 \times 11''.13$ ) and (d) NGC 4710 ( $5''.50 \times 5''.16$ ). NGC 4470 and NGC 4710 are H II nuclei.

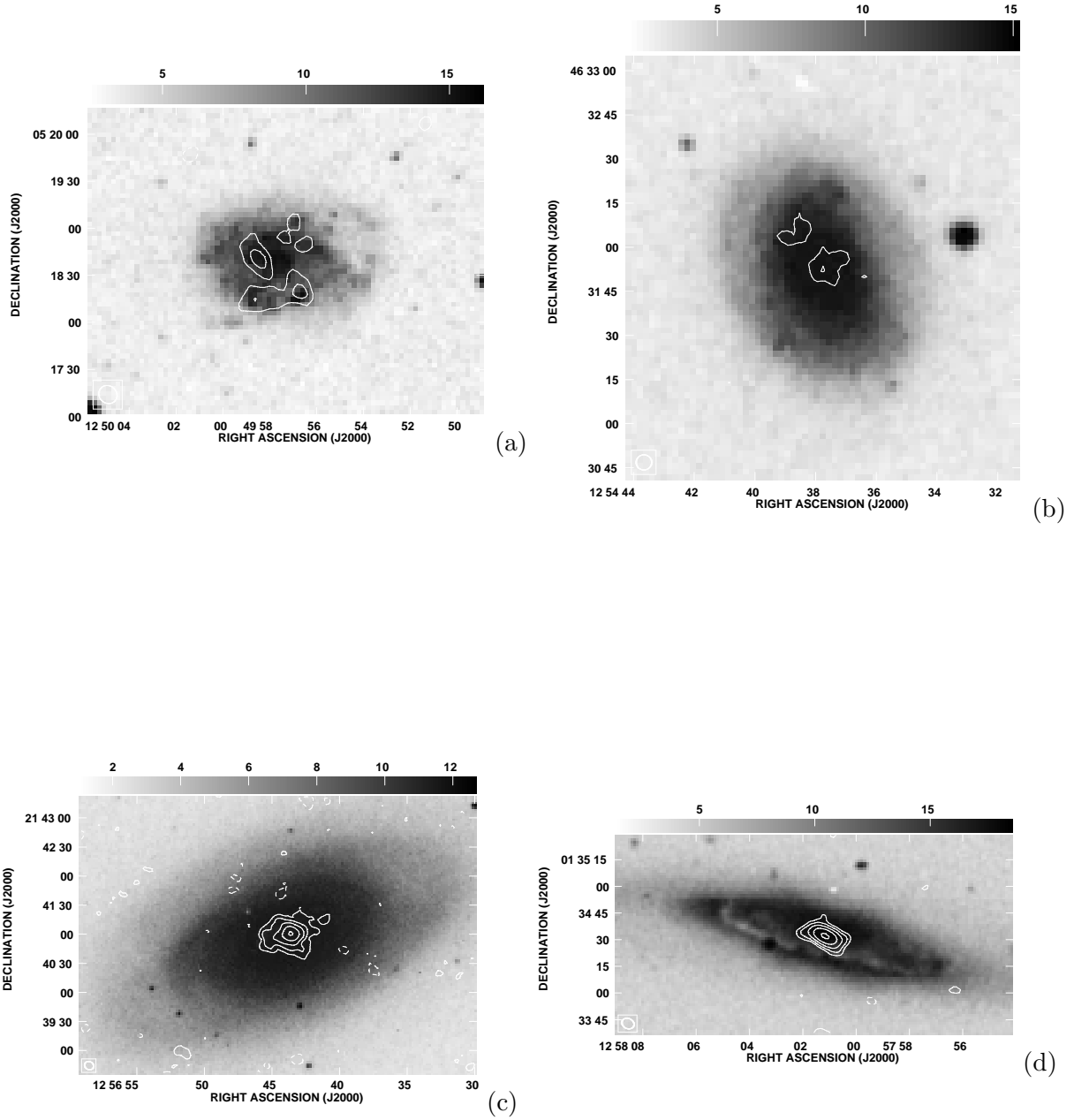


Fig. 5.— As in Figure 1. (a) NGC 4713 ( $12''.12 \times 10''.95$ ), (b) NGC 4800 ( $5''.28 \times 5''.15$ ), (c) NGC 4826 ( $9''.62 \times 8''.26$ ) and (d) NGC 4845 ( $7''.08 \times 5''.69$ ). NGC 4845 is an H II nucleus.

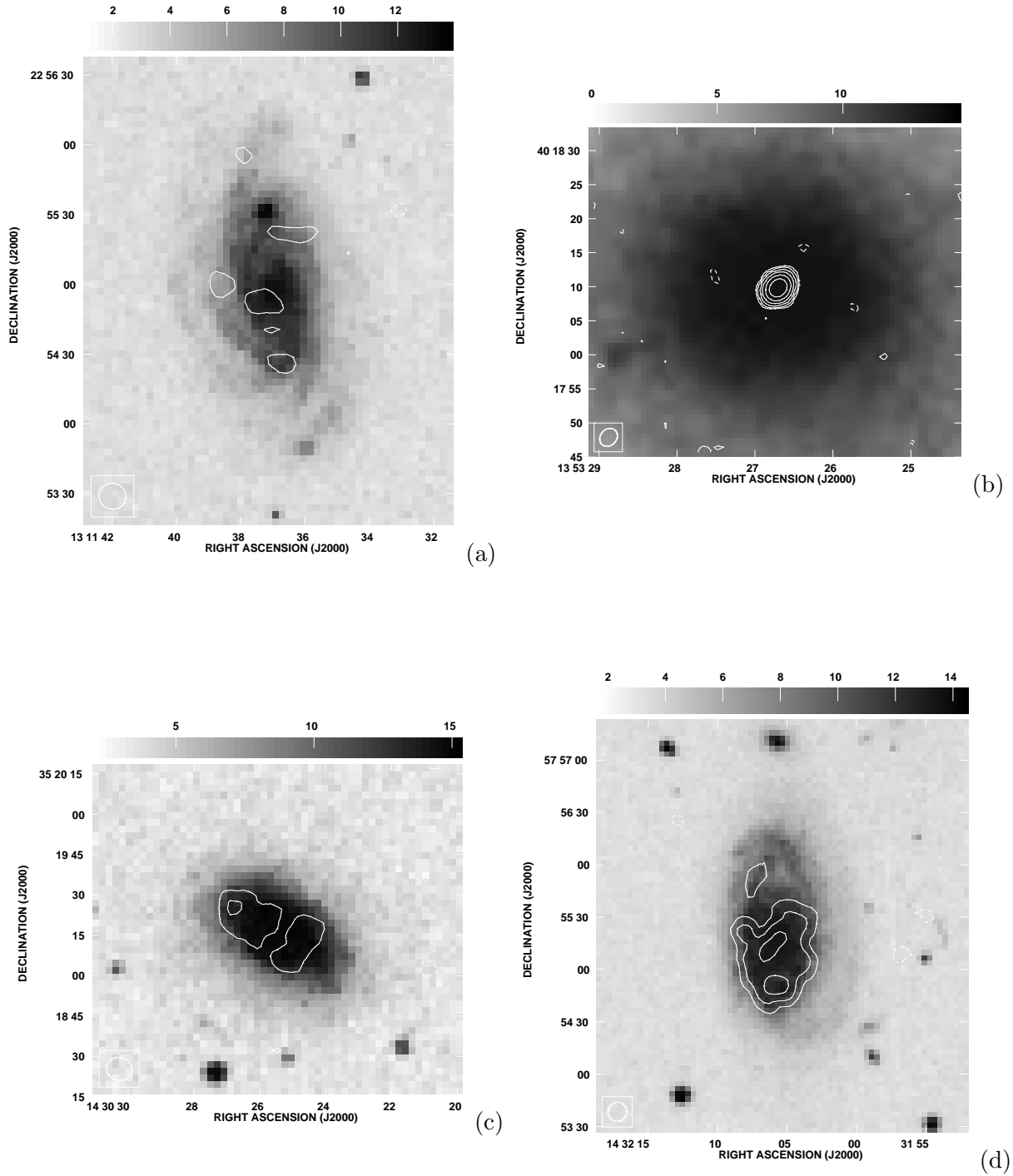


Fig. 6.— As in Figure 1. (a) NGC 5012 (11''59 × 11''18), (b) NGC 5354 (2''84 × 2''37), (c) NGC 5656 (9''54 × 8''39) and (d) NGC 5678 (11''09 × 10''75).

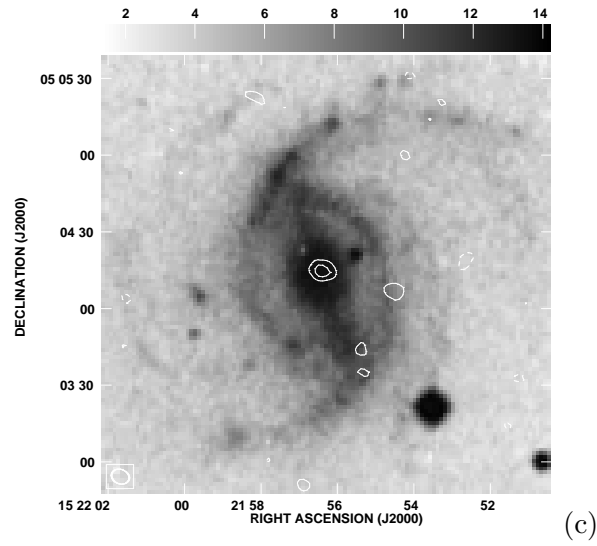
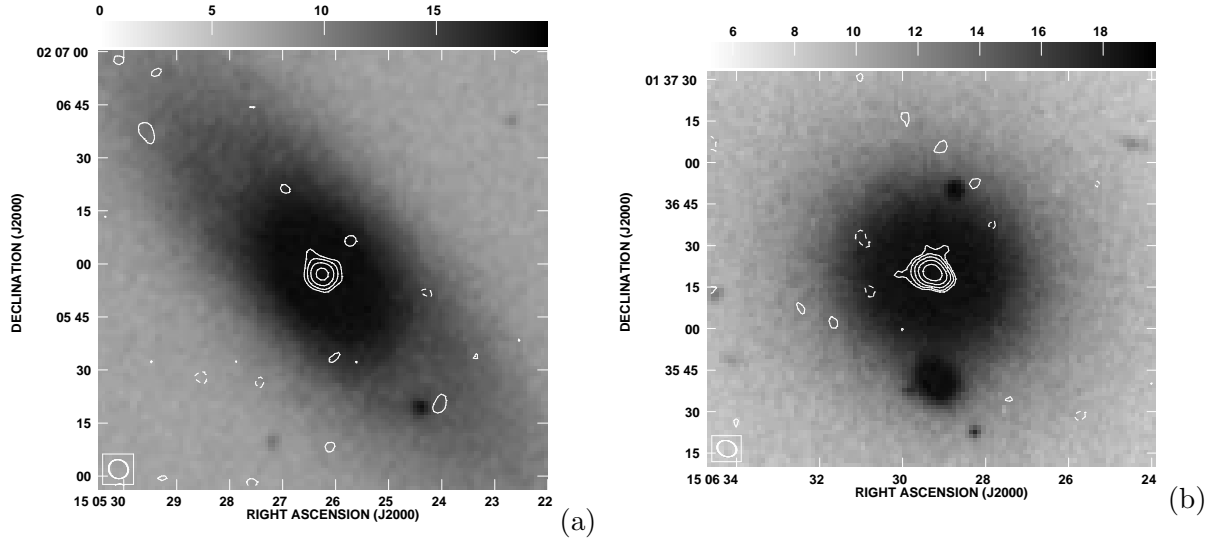


Fig. 7.— As in Figure 1. (a) NGC 5838 ( $5''.62 \times 5''.23$ ), (b) NGC 5846 ( $7''.06 \times 5''.67$ ) and (c) NGC 5921 ( $7''.12 \times 5''.63$ ).